European Polymer Journal xxx (2016) xxx-xxx

Contents lists available at ScienceDirect

European Polymer Journal

journal homepage: www.elsevier.com

Nucleation induced by "Short-Term Pressurization" of an undercooled isotactic polypropylene melt

E.M. Troisi [a, b], S. Formenti [c], F. Briatico-Vangosa [c, *], D. Cavallo [d, *], G.W.M. Peters [a, b, *]

[a] *Department of Mechanical Engineering, Materials Technology Institute, Eindhoven University of Technology, P.O. Box 513, 5600 MB Eindhoven, The Netherlands*
[b] *Dutch Polymer Institute (DPI), P.O. Box 902, 5600 AX Eindhoven, The Netherlands*
[c] *Dipartimento di Chimica Materiali e Ingegneria Chimica G. Natta, Politecnico di Milano, piazza Leonardo da Vinci 32, 20133 Milano, Italy*
[d] *Department of Chemistry and Industrial Chemistry, University of Genova, Via Dodecaneso 31, Genova, Italy*

ARTICLE INFO

Article history:
Received 19 September 2016
Received in revised form 25 October 2016
Accepted 1 November 2016
Available online xxx

ABSTRACT

Nucleation of semi-crystalline polymers is very sensitive to perturbations of the melt state. In contrast to the case of flow, the influence of pressure changes on nucleation has been almost neglected so far. In this work we explore the effect of the pressure history on isotactic polypropylene crystallization by applying a brief step-like increase of pressure to the undercooled melt. Using dilatometry and synchrotron X-ray diffraction, an enhancement of crystallization kinetics proportional to the magnitude of the pressure pulse is revealed. This acceleration is linked to an increase of the number of active nuclei after the short term pressurization, as confirmed by ex-situ optical microscopy observations. Up to an order of magnitude increase in nucleation density is found, for pressure pulses around 600–700 bar. The pressure-induced nucleating effect is interpreted in the light of classical nucleation theory; although a non-classical "barrier-less" nucleation mechanism is also envisaged.

1. Introduction

The crystallization kinetics of semicrystalline polymers is often tailored by acting on the nucleation stage, for instance with purposely added nucleation catalysts. Controlling the crystallization in these materials is of paramount importance from the technological point of view: the degree of crystallinity and morphology determines their properties (e.g., optical, mechanical), while the crystallization rate often dictates the processing times.

Nucleation kinetics is controlled by the degree of undercooling experienced by the melt, i.e., the distance between crystallization and equilibrium melting temperatures. This parameter sets the height of the free energy barrier and the critical size that a given crystalline cluster should overcome in order to be able to spontaneously grow to macroscopic size [1]. On the other hand, the undercooling is related to the thermodynamic crystallization conditions, such as the pressure.

However, polymer nucleation proved to be also affected by a variety of external perturbations of the equilibrium conditions of the system. For instance, the number of active nuclei at the crystallization temperature is related to the initial melt annealing stage when relatively mild melting conditions are applied, an effect known as self-nucleation [2–8]. Moreover, nucleation kinetics is also affected by the adopted cooling/heating rate from the melt or glass, respectively [9–11]. Perturbations by external force fields, such as electric fields [12–15] or shear and elongational flows [16–23], profoundly alter the process as well.

The case of flow-induced nucleation is surely the best known in polymer crystallization, and that with the most remarkable effect. Nucleation densities can increase of several (e.g., 2–6) orders for magnitude with respect to quiescent conditions, depending on the intensity of the flow field [17,19].

* Corresponding authors at: Department of Mechanical Engineering, Materials Technology Institute, Eindhoven University of Technology, P.O. Box 513, 5600 MB Eindhoven, The Netherlands (G.W.M. Peters).
Department of Mechanical Engineering Materials Technology Institute Eindhoven University of Technology P.O. Box 513 5600 MB Eindhoven The Netherlands
Email addresses: francesco.briatico@polimi.it (F. Briatico-Vangosa); dario.cavallo@unige.it (D. Cavallo); g.w.m.peters@tue.nl (G.W.M. Peters)

http://dx.doi.org/10.1016/j.eurpolymj.2016.11.001
0014-3057/

While early studies of flow-induced crystallization were conducted under continuous shear, a landmark in the understanding of the phenomenon was reached with the introduction of the so-called short-term shear protocol by Janeschitz-Kriegl and Eder [16]. According to this procedure, a brief pulse of shear is imposed to the undercooled melt, with a variable duration which is always much shorter than the characteristic crystallization time. The basic idea is that, in this way, flow only affects the nucleation stage, while the growth of polymer crystals occurs under quiescent conditions. As such, the effect of flow variables on the sole nuclei production can be easily investigated. Notice, however, that for sufficient strong flow this assumption doesn't hold anymore [24,25].

Although the occurrence of high pressures is common practice in polymer melt processing, for instance in injection molding, the study of pressure-induced nucleation and crystallization received much less attentions. Referring exclusively to the works on isotactic polypropylene (i-PP), of relevance to the present study, the large majority of the experiments were carried on under constant pressure during crystallization [26–32]. The observed increase in nucleation density with increasing pressure is understood and described taking into account the higher undercooling [26–28] due to the shift of the equilibrium melting temperature under pressure (dT_m/dp is about 30 °C/kbar for i-PP).

As demonstrated for flow-induced crystallization by using a flow-pulse, the application of a short-term pressurization approach can be essential to understand the influence of pressure perturbations on the nucleation process, besides the trivial undercooling effect in constant pressure experiments. Moreover, this protocol would also be of practical relevance, since step-like pressure changes during polymer solidification are actually met in real processing, i.e., in the packing stage of injection molding [33,34].

To the best of our knowledge, only one study adopting this experimental protocol (analogous to the short-term shear experiments) exists at present [35]. In this work, Zhang et al. did not detect any effect of pressure pulses of various duration at different temperatures (with a pressure of 800 bar) on the subsequent non-isothermal crystallization temperature. They concluded that either no pressure-induced nucleation precursors are formed during the pressure pulse, or that possibly formed nuclei immediately dissolve back in the melt when the extra-pressure is released.

In this study we designed an improved short-term pressure protocol to detect even minute changes in the nucleation density of the system upon application of pressure pulses. The key feature is the choice of a slow isothermal crystallization at relatively low undercooling, so that the nucleation density of the unperturbed system is low enough, and even mild effects of pressure pulses on the concentration of active nuclei could be highlighted. An enhancement of nucleation density upon short-term pressurization of an undercooled i-PP melt is actually observed, and its origin is discussed in light of the classical nucleation theory. Furthermore, the possible existence of an atypical mechanism of nuclei formation is also hypothesized.

2. Experimental

2.1. Material

The material elected for this investigation is a commercial isotactic polypropylene (Borealis HD601CF) used in several other studies [21,24,25] with a weight average molecular weight M_w of 365 kg/mol and a polydispersity index M_w/M_n of 5.4. The nominal melting point (evaluated from differential scanning calorimetry heating run at 5 °C/min) is 166 °C.

2.2. Dilatometry

The experiments were performed with a commercial PVT confining fluid dilatometer (Gnomix Inc.). Upon calibration, this type of apparatus measures relative specific volume variations with a precision of 0.0004 cm^3/g. For the dilatometric measurements, approximately 1 g of iPP pellets was used as received. Mercury was employed as confining fluid.

Isobaric cooling (2 °C/min) and heating (5 °C/min) experiments were performed at 100, 300, 600 and 900 bar to evaluate the linear dependence of melting and crystallization temperatures on the applied pressure. These were found to be dT_m/dp = 32 °C/kbar and dT_c/dp = 27 °C/kbar, respectively, in good agreement with previous literature data [26,27,36]. The relative specific volume vs. temperature curves are collected in the Supporting Information, Fig. S1.

Short-term pressure pulse experiments were carried out according to the protocol depicted in Fig. 1: the sample was heated up to 220 °C at 5 °C/min under a pressure of 100 bar and kept at 220 °C for 10 min to erase the possible memory of previous thermo-mechanical history on subsequent crystallization. Then, it was isobarically (100 bar) cooled at 2 °C/min to the chosen isothermal crystallization temperature, T_c = 145 °C. After temperature stabilization (about one minute), the pressure was increased from the reference value of 100 bar (P_c) to different levels (P_{pulse}) in the range 200–700 bar. The pressure was kept constant for 1 min, and then released back to 100 bar. Both pressure increase and decrease were completed in less than 10 s. The pressures applied during the pulse were varied in a random fashion to prevent any systematic error in the dilatometry measurements when the same sample was used for different experiments. Note that the pressurization time (60 s) is much shorter than the typical crystallization time at 145 °C and 100 bar (crystallization half-times of the order of 20,000 s). Hence, the definition of short-term pressure pulse experiment applies. After the pressure pulse, the relative decrease of specific volume due to crystal-

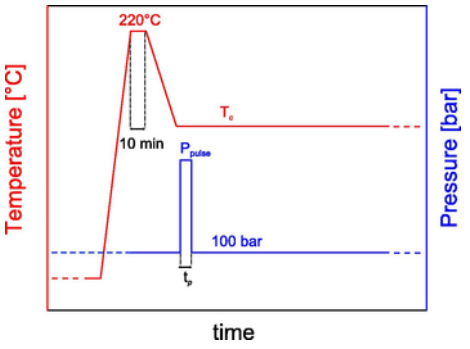

Fig. 1. Adopted experimental protocol. The crystallization temperature, T_c, and the duration of the pressure pulse, t_p, were 145 °C and 60 s for dilatometry, and 140 °C and 30 s for in situ X-ray experiments, respectively.

lization was followed in time at T_c and P_c. The repeatability of the experiments was assessed from multiple crystallization measurements for selected values of pressure pulses.

The relative variations of specific volume were then converted to absolute specific volume, v, by equating the initial value to the value for the specific volume of isotactic polypropylene at 100 bar and 145 °C measured by He and Zoller [26].

The degree of space filling ($\xi(t)$) as a function of time could then be obtained from the specific volume evolution by using:

$$\xi(t) = \frac{v_0 - v(t)}{v_0 - v_\infty}; \tag{1}$$

where $v(t), v_0$ and v_∞ are the values of the specific volume at a given time t, at the initial state and at the end of crystallization, respectively.

2.3. In-situ X-ray measurements

2.3.1. Pressure cell

Structural and morphological evolutions after pulses of different pressures were investigated by combining in situ synchrotron X-ray measurements and a pressure cell adapted from a multi-pass rheometer (MPR). This experimental setup was used in previous works as a slit flow device and it has been described in detail elsewhere [37–39], recent modifications allow to apply and carefully control pressures up to 1000 bar on polymer specimens. The sample (120 × 6 × 1.5 mm) is confined between two hydraulically driven pistons: pressurization and de-pressurization can be imposed by moving the pistons towards or away from each other, and the set values of pressure are controlled by mean of two pressure transducer positioned near each of the pistons. Cooling occurs by pumping a cooling medium through the cell (resulting in an average cooling rate of 7 °C/min) and a diamond window placed in the middle of the pressure cell allows on-line scattering measurements (Fig. 2). The effect of shear flow, due to the movement of the piston and compressibility of the material, is confined to the region of the pressure cell close to the pistons, far away from the X-ray observation window, and does not affect the measurements. Therefore, all the observed effect on crystallization kinetics can only be ascribed to pressure changes. To confirm this, we show a clearly isotropic 2D SAXS pattern collected at the end of the isothermal crystallization at 145 °C and a pulse of 700 bar in the Supporting Information, Fig. S2.

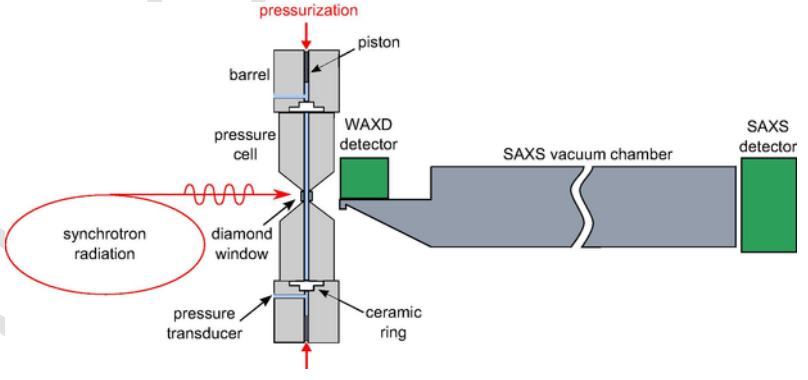

Fig. 2. Schematic drawing of the pressure cell combined with synchrotron WAXD/SAXS measurements.

The short-term pressure pulse protocol was used also for this set of X-ray experiments (Fig. 1), but experimental conditions were modified due to time limitations at the synchrotron facility. After erasing of the previous thermo-mechanical history at 220 °C for 10 min the sample was cooled to an isothermal crystallization temperature of 140 °C, which is lower with respect to the dilatometry experiments. This resulted in faster crystallization kinetics and, as a consequence, the duration of the pressure pulse was shortened accordingly (30 s instead of 60 s), to prevent the material from crystallizing during the pressurization step. In this way, although the isothermal crystallization temperature and the duration of the pulse were changed for this set of experiments, the purpose of separating the nucleation stage from the crystal growth step is still fulfilled and the results from the two different techniques will be compared throughout this paper. Note that in this case the sample was changed for each experiment.

2.3.2. In-situ Xray measurements and data analysis

Time resolved Small Angle X-ray Scattering and Wide Angle X-ray Diffraction (SAXS and WAXD) measurements were carried out at beamline BM26B [40] at the European Synchrotron Radiation Facility (ESRF) in Grenoble with a X-ray wavelength λ = 1.033 Å. Simultaneous acquisition of SAXS and WAXD patterns was performed using a Pilatus 1 M detector 981 × 1043 pixels of 172 μm × 172 μm, at a distance of 6.47 m from the pressure cell) and a Pilatus 300 K detector (1472 × 195 pixels of 172 μm × 172 μm, at a distance of 0.21 m from the sample cell), respectively. The detectors were triggered by an electric TTL pulse at the start of the displacement of pistons during the pressure pulse, in order to synchronize data acquisition. The structure evolution during the 30 s pressure pulse was monitored using an exposure time of 5 s, the following 1200 s of isothermal and isobaric crystallization were followed with an acquisition time for 30 s (10 s exposure time and 20 s waiting time). The distance and tilt angle of the SAXS and WAXD detectors were calibrated using rat tail collagen and α-Al_2O_3 (α-aluminum oxide) standard powder, respectively. After correction for the background and air scattering, all X-ray images were normalized for synchrotron beam fluctuations using an ionization chamber placed before the sample, and for the sample absorption using a photodiode placed on the beamstop. In addition, X-ray images of a completely molten sample at 140 °C were collected before the pressure pulse and used as amorphous scattering pattern in the crystallinity evaluations. 2D WAXD and SAXS images were processed with the software package FIT2D to obtain 1D intensity profiles as a function of the scattering angle (2θ) for WAXD and of the scattering vector $\left(q = \frac{4\pi}{\lambda}\sin\theta\right)$ for SAXS.

Crystallinity was calculated after deconvolution of the total intensity scattered by the crystalline ($A_{crystal}$) and amorphous ($A_{amorphous}$) domains using:

$$X_c = \frac{A_{crystal}}{A_{crystal} + A_{amorphous}} \times 100 \tag{2}$$

The degree of space filling was obtained from crystallinity evolution using:

$$\xi(t) = \frac{X_c(t) - X_c^0}{X_c^\infty - X_c^0} \tag{3}$$

where $X_c(t)$ is the measured values of the crystallinity at a given time t, X_c^0 the values before the pressure pulse and X_c^∞ the values at the end of the crystallization process. The relative amount of crystals in the γ and α phases was evaluated from the time-resolved X-ray diffraction profiles, as suggested by Turner-Jones et al. [41] and Murthy and Minor [42], by measuring the ratio between the intensity of the $(1\ 1\ 7)_\gamma$ reflection at 2θ = 13.2°, typical of the γ phase, and the $(1\ 3\ 0)_\alpha$ reflection at 2θ = 12.1°, typical of the α phase. The fraction of the two polymorphs crystals is thus given by: $f_\gamma = I(117)_\gamma/[I(130)_\alpha + I(117)_\gamma]$ and $f_\alpha = I(130)_\alpha/[I(130)_\alpha + I(117)_\gamma]$. The intensities of $(1\ 1\ 7)_\alpha$ and $(1\ 3\ 0)_\gamma$ reflections were evaluated from the areas underneath the corresponding diffraction peaks above the diffuse amorphous halo in the X-ray diffraction profiles.

The long period (L_p) was calculated from the Lorentz corrected 1D SAXS intensity profiles by simple application Braggs law: $L_p = 2\pi/q^*$, where q^* is the value of the scattering vector corresponding to the maximum of the correlation peak of the integrated intensity. The lamellar thickness (l_c) was estimated as $l_c = L_p \times X_c$, where X_c is the crystallinity evaluated from WAXD.

2.4. Polarized optical microscopy

The samples crystallized after the application of different pressure pulses were recovered from the pressure cell and analyzed ex-situ using polarized optical microscopy. Optical micrographs were taken under crossed polars, from samples slices of 50 μm thickness cut parallel to the X-ray direction at 4 different positions along the slit length.

The number of spherulites per micrograph, N_A, was counted in the visible field. Knowing the observed area, A_{mic}, the approximate nucleation density per unit volume was evaluated according to Janeschitz-Kriegl et al. [19,43]:

$$N_{POM} = \left(\frac{N_A}{A_{mic}} \right)^{3/2} \tag{4}$$

3. Results

3.1. Dilatometry

The time evolutions of the specific volume after pressure pulses of different magnitude are presented in Fig. 3 on a linear (a) and on a logarithmic scale (b), to emphasize the changes of crystallization kinetics and the recovery of specific volume after the pulse, respectively. As expected, the specific volume, v, gradually decreases with time from the value of a completely amorphous iPP melt to a final constant value, v_{fin} = 1.1522 cm^3/g, indicating the end of crystallization. Assuming specific volumes of 1.0695 cm^3/g [44] and 1.2657 cm^3/g [26] for fully crystalline and fully amorphous iPP at 145 °C, the final crystallinity degree can be evaluated as $x_c = (v_{am} - v_{fin})/(v_{am} - v_{cryst})$. A value of 0.58 is found, in agreement with the data obtained by van Drongelen et al. after crystallization of the same material in non-isothermal conditions [45].

Two main observations can be made on the results of the dilatometry experiments: (1) the volume contraction associated to the phase transition occurs at shorter and shorter times with increasing the magnitude of the pressure applied during the pulse, and (2) the specific volume completely recovers after the pulse to the value of the complete amorphous sample (1.2657 cm^3/g) only for P_{pulse} lower than 500 bar. For pressures pulses ranging from 500 to 700 bar, a small decrease in the specific volume is observed after the de-pressurization at 100 bar, indicating partial crystallization during the 60 s spent at high pressure. However, the crystallinity after the pulse is estimated to be less than 1%, i.e., it can be safely assumed that most of the crystal growth takes place after the pressure pulses. The space filling evolution for the set of dilatometry experiments evaluated by using Eq. (1) is presented in Fig. 4, together with the crystallization half-times ($t_{1/2}$) as a function of the pressure applied during the pulse. As already evident from the specific volume time evolutions, crystallization kinetics is accelerated and a monotonic decrease of the crystallization half-time with increasing P_{pulse} is observed. A pulse of 700 bar reduces by more than half the value of the crystallization half-time, with respect to the reference value (no pulse applied). We note that the pressurization/depressurization steps cause a consecutive raise and drop of the polymer temperature. Temperature variations as big as 1.5–2 °C were measured for the experiment in which the highest pressure pulse (700 bar) was applied. This transient effect lasted at most 400 s, before the set isothermal crystallization temperature was reached. This temperature undershoot, one order of magnitude shorter than the crystallization half-time at 145C and 100 bar, did not cause any appreciable effect on crystallization kinetics/nucleation, which is found to be dominated by the effect of the pressure pulse. Indeed, the crystallization half-time for an isothermal crystallization at

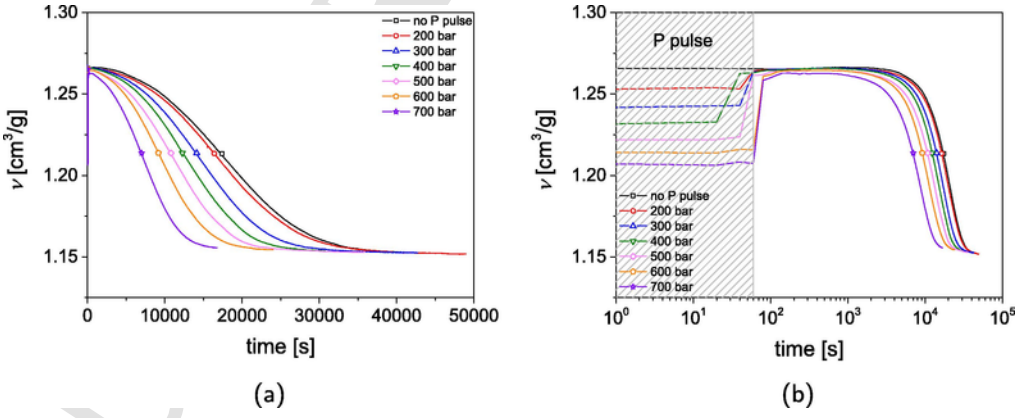

Fig. 3. Time evolution of the specific volume 145 °C after pulses of different pressure plotted on a linear (a) and a logarithmic scale (b).

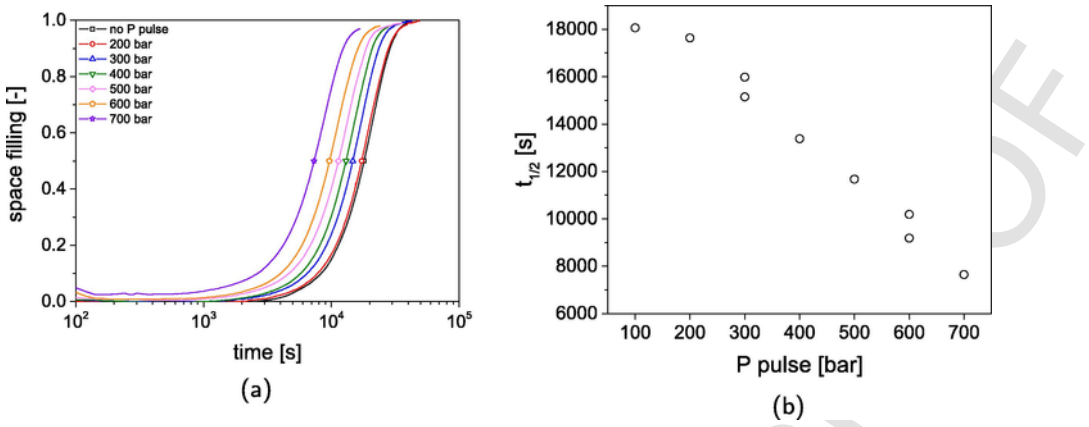

Fig. 4. Time evolution of the space filling at 145 °C after pulses of different pressure (a) and related crystallization half-time (b) obtained from dilatometry experiments. The value of 100 bar corresponds to the isobaric reference experiment.

143 °C measured with the same experimental technique, was found to be around 15,000 s, more the double of the $t_{1/2}$ measured for the experiment with the pulse of 700 bar.

3.2. In-situ X-ray measurements

The acceleration of crystallization kinetics after pulses of pressure deduced from dilatometric experiments is independently confirmed by the on-line X-ray measurements. The time evolution of crystallinity for experiments performed using the pressure cell is reported in Fig. 5a. Crystallization kinetics becomes increasingly faster, with increasing the pressure applied during the pulse and, for the experiments with a pulse of 600 and 700 bar, a detectable partial crystallization is observed already during the 30 s at higher pressure. Similar results were found from the independent analysis of the SAXS invariant (see Fig. S3 in Supporting Information). The fraction of material crystallized immediately after the pulse for these two experiments is 1.5 and 3% respectively, while the final values of crystallinity is about 60% for all the experiments, in agreement with the value derived from dilatometry, despite the different experimental conditions. Once more, we underline that the great majority of crystal growth occurs upon de-pressurization (at 100 bar), and this confirms the effectiveness of our devised short-term pressure protocol in separating the nucleation stage from bulk sample crystallization. As expected due to the crystallization under non-atmospheric pressure, some amount of γ phase develops, next to the usual monoclinic α polymorph. The evolution of the relative amount of the two different phases is not appreciably affected by the pressure pulses (Fig. 5b). The formation kinetics of both phases is speeded up with increasing the pressure during the pulse, but the final relative amount remains the same for all the experiments, independently of the magnitude of the pressure pulse. As well known from previous works on polypropylene crystallization under pressure [45,46], in these conditions of temperature and pressure the α-phase growth rate is higher than the one of

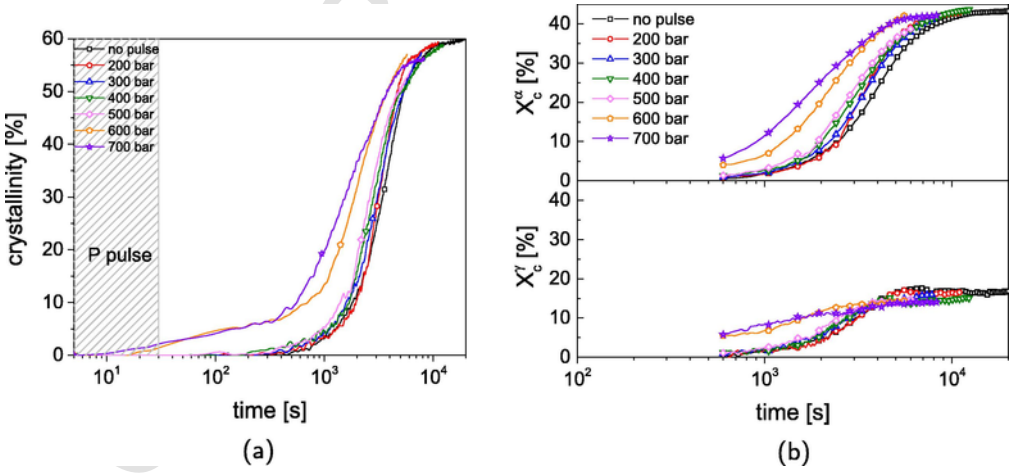

Fig. 5. Time evolution of the crystallinity (a) and of the α and γ phase contents (b) for the experiments performed at 140 °C coupling the pressure cell with in situ X-ray.

the γ-phase, and therefore the first polymorph largely prevails at the end of the crystallization. We note that the ratio between α and γ crystallinity in a bulk sample is a function of the ratio between the respective growth rates. We deduce that the growth process of the two polymorphs is apparently not influenced by the short transient at higher pressures. In agreement with recent observations on iPP crystallization under shear flow [23], it is reasonable to hypothesize that the growth rate returns immediately to the value characteristic of the thermodynamic boundary conditions (T_c, P_c), as soon as the perturbation (flow or pressure in this case) is removed.

Further support to this hypothesis is provided by the final values of the lamellar thickness, reported as a function of the pressure applied during the pulse in Fig. 6. The final value of lamellar thickness is 14 nm, independently from the value of P_{pulse}. Clearly, the short time experienced by the material at higher pressure does not have a clear effect on the final structure and morphology, these being affected only by the actual temperature and pressure at which the crystal growth occurs.

4. Discussion

As stated before, our approach aims to separate nucleation during a sharp and short increase of the pressure from the subsequent crystal growth, which, in these experiments, mainly occurs after the pressure is returned to the chosen reference value (100 bar). The time evolution of the degree of space filling is usually described by using the Avrami-Kolmogorov equation [47]:

$$\xi(t) = 1 - \exp[-Ct^n] \tag{5}$$

where C is the overall rate of crystallization and n the Avrami exponent, which reflects the crystal dimensionality and the type of nucleation (sporadic or heterogeneous, i.e. predetermined). For a heterogeneously nucleated polymer melt with spherulites growing in 3 dimensions Eq. (5) becomes:

$$\xi(t) = 1 - \exp\left[-\frac{4}{3}\pi\, N(T,P)\, G(T,P)^3\, t^3\right] \tag{6}$$

where both nucleation density N and linear growth rate G are a function of temperature and pressure only. Avrami exponent between 2 and 3 are observed in the Avrami plots of the dilatometry and X-ray experiments, shown in the Supporting Information, Fig. S4. He and Zoller [26] already observed a decrease in the Avrami exponent during isothermal crystallization of iPP at elevated pressure. For the aim of simplicity of our analysis, we consider the Avrami exponent equal to 3, as a reasonable approximation (see Fig. S4, the slope is actually very close to 3. Small deviations, observed especially for the experiments in which crystallization already happens during the pulse, can be explained by a not constant growth and nucleation, for a short time, during the application of the pulse). On the basis of the recovery of the specific volume after the pressure pulses (Fig. 3b) we can safely assume that most of the growth process occurs after de-pressurization at 100 bar. Therefore the growth rate can be considered constant for all the performed experiments, since crystallization always occurs under the same isothermal and isobaric conditions. From the experimentally determined values of crystallization half-time, $t_{1/2}$, we can estimate the number of nuclei that act as crystallization centers for each experiment:

$$N = \frac{3\ln(2)}{4\pi\,(G\,t_{1/2})^3} \tag{7}$$

It follows that the observed decrease of $t_{1/2}$ with increasing the pressure during the pulse (Fig. 4b) can be related to an in-

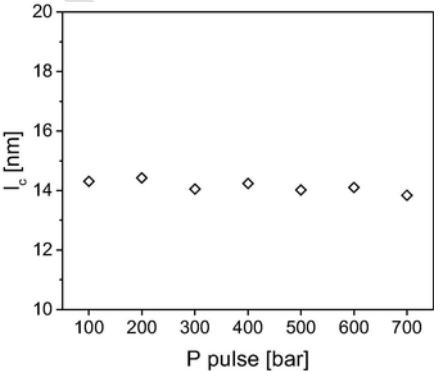

Fig. 6. Final values of the lamellar thickness as a function of the applied pressure pulse at 140 °C. The value of 100 bar corresponds to the isobaric reference experiment.

creased nucleation density. In other words, the temporary increase of pressure during the pulse causes the formation of extra nuclei that can survive upon de-pressurization and subsequently grow into crystals.

Further support to this hypothesis is provided by the ex-situ microscopy analysis of the samples collected after the experiments in the pressure cell. Micrographs of samples crystallized after different pressure histories (i.e., without pulse, and with pressure pulses of 300 and 500 bar) are shown in Fig. 7. The characteristic spherulitic morphology can be appreciated with the average spherulites dimensions decreasing with increasing the magnitude of the pressure pulse, indicating a higher nucleation density. Besides, rectilinear boundaries between impinged spherulites are observed, as expected for predetermined nucleation [48]. The absolute value of nucleation density could be evaluated from the crystallization half-times using Eq. (7) and values of growth rates from literature. [45] However, for a relative comparison it is sufficient to calculate the ratio between the nucleation density after a given pulse of pressure (N^{Ppulse}) and the reference value (without pressure pulse, $N^{nopulse}$):

$$\frac{N^{Ppulse}}{N^{nopulse}} = \left(\frac{t_{1/2}^{nopulse}}{t_{1/2}^{Ppulse}} \right)^3 \tag{8}$$

The nucleation densities ratios from dilatometry, X-ray experiments and optical micrographs are presented in Fig. 8. Data from the three different techniques show good agreement, although the dilatometry and the X-ray experiments were performed in different experimental conditions. Therefore the order of magnitude of the nucleation increase by pressure pulses can be considered accurate. The absolute values of nucleation densities estimated from POM micrographs are 9.58×10^{10} and 1.04×10^{12} nuclei/m^3, for the reference experiment at 100 bar and the experiment with a pulse of 600 bar, respectively (for quantitative estimation of nucleation densities by POM see Fig. S6 in Supporting Information).

The increase in the concentration of athermal nuclei can be interpreted in light of the kinetic theory of nucleation [4,49]. The rate of formation of ordered clusters of a given size is governed by the kinetics of association and dissociation of single elements, for instance chain stems in the case of polymers. Under these conditions a Boltzmann-like equilibrium distribution of cluster size (CSD) results: the probability of finding clusters of size r decreases with increasing their dimension. When the temperature is lowered below T_m crystallization can occur and the equilibrium CSD is modified until a "steady-state" situation sets in [4]. The number of active nuclei at the crystallization temperature is given by the concentration of clusters with sizes larger

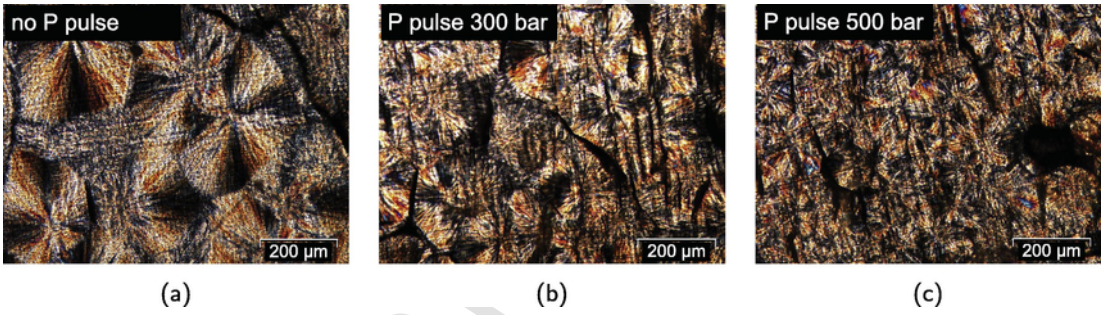

Fig. 7. Optical micrographs of microtomed samples after isothermal crystallization at 140 °C and 100 bar (a) and after crystallization in the same conditions and previous application of pressure pulses of 300 (b) and 500 bar (c).

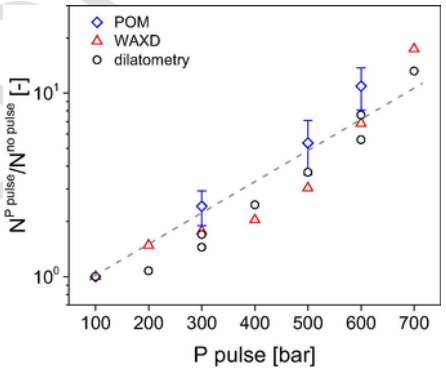

Fig. 8. Ratio between the nucleation density with and without pressure pulse (100 bar), evaluated with different experimental methods (dilatometry at 145 °C, WAXD and polarized optical microscopy at 140 °C), as a function of the pressure value during the pulse. The dashed line is a guide to the eye.

than the critical value (r^*) determined by the undercooling dependent free energy barrier for nucleation (ΔG^*); i.e., by the area underneath the CSD function for $r > r^*$.

The results of our short-term pressurization experiments indicate that the number of aggregates with a supercritical size at T_c and $P_c$after the pressure pulse is higher than the reference situation. thus the "steady-state" cluster size distribution function is perturbed with respect to the original situation. This is schematically depicted in Fig. 9. The CSD of the perturbed melt has an enhanced concentration of large-size clusters, with a correspondent depletion of small elements resulting in an increase in the number density of supercritical clusters (the difference between the red and black hatched areas in the plot of Fig. 9).

Clearly, several clusters increased their dimensions during the short pressurization stage: this cluster growth can be interpreted in light of the classical nucleation theory. Aggregates that are large enough to overcome the Gibbs free energy barrier for nucleation are kinetically stable, i.e., they spontaneously grow to large size crystals, since their growth is associated with an overall decrease of the free energy of the system. Both the critical cluster size (r^*) and the height of the free energy barrier (ΔG^*) depend on the undercooling, which in turns depend on pressure because of the well-known Clausius-Clapeyron equation which relates melting temperature to pressure [50]: an increase of pressure corresponds to an increase of the undercooling at constant crystallization temperature. Therefore, both r^* and ΔG^* are decreased during the applied pressure pulse, with respect to their values at T_c and P_c. This scheme also apply to heterogeneous nucleation, whereas the magnitude of the free energy barrier at a given undercooling is reduced compared to the homogeneous case, by the effect of the nucleating substrate-polymer crystal favorable interaction.

This is schematically shown in Fig. 10, where the free energies of nucleation are plotted as a function of the cluster size for a crystallization temperature of 145 °C and two different pressures (100 and 500 bar) according to the simplified nucleation model [51,52] described in the Supporting Information and assuming a pressure-dependence of the i-PP T_m^0 (dT_m/dp) of 32 °C/kbar.

Upon application of the higher pressure several subcritical clusters will instantaneously become supercritical (step 1 of the pathway in Fig. 10), and will therefore achieve kinetic stability and undergo further growth (thermodynamically favorable situation, step 2 in Fig. 10). Moreover, the lower energy barrier will also increase the frequency of other embryos-to-nuclei transfor-

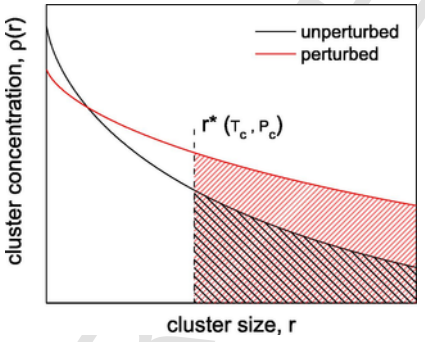

Fig. 9. Concentration of clusters as a function of their size: reference steady-state cluster size distribution (black line) and CSD after the pulse of pressure (red line). The hatched areas represent the number of aggregates with supercritical size under the given thermodynamic conditions (T_c, P_c) in the two situations. (For interpretation of the references to color in this figure legend, the reader is referred to the web version of this article.)

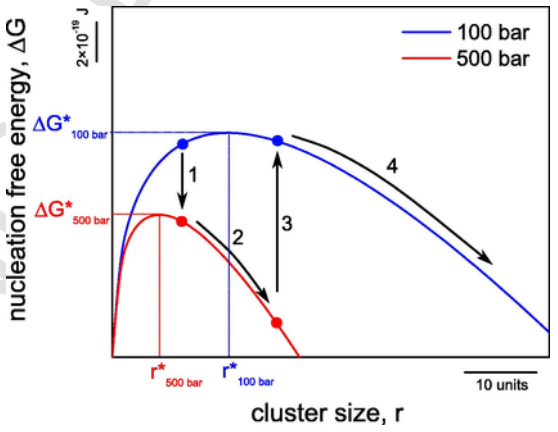

Fig. 10. Free energy of nucleation as a function of the cluster size at T_c = 145 °C, for different values of applied pressure (pressures of 100 and 500 bar).

mations, due to spontaneous fluctuations in the clusters size. Although new nuclei can develop during the time spent at P_{pulse}, their growth into macroscopic size crystals is still limited, as testified by the negligible crystallinity increase in the pressurization stage observed with dilatometry or X-ray measurements (Figs. 3b and 5a). Once pressure is brought back to the reference value of 100 bar (step 3 in Fig. 10), some of the clusters might have already grown to such an extent that they are supercritical also in the new conditions (T_c, P_c), and can therefore continue their growth during the isothermal crystallization (step 4 in Fig. 10). The pathway in the free energy-cluster size landscape highlighted in Fig. 10 can account for the measured increase in nucleation density induced by the pressure pulse.

Obviously, the probability of finding supercritical clusters after de-pressurization (at T_c and P_c) is inversely proportional to the height of the free energy barrier for nucleation at the pressurization stage, ΔG^*_{Ppulse}. Since this barrier will decrease with the magnitude of the pressure pulse applied, the obtained nucleation density increases accordingly, as clearly shown in Fig. 8. This increase is thus directly related to the pressure dependence of T^0_m. The above described mechanism of cluster growth is surely active during short-term pressurization experiments. However, the existence of a different, "barrier-less" nucleation mechanism, simultaneously active with this first one, can also be hypothesized. Indeed, a non-classical pathway for nuclei formation, governed by melt dynamics, has been proposed by Kornfield et al. [53] for the flow-induced nucleation of isotactic polypropylene.

Following this idea, it appears reasonable that during the densification of the material at P_{pulse}, while polymer chains segments are brought closer to each other, some of them will be at a reciprocal distance favorable to their interactions, i.e., similar to the one that the chains possess in the crystalline lattice. When the pressure is released, such clusters generated in a non-classical way will probably not dissolve, if the gain in stability due to improved segmental interactions overcomes the effect of thermal motions which tends to randomize them.

If we compare our observations with previous literature results reported by Zhang et al. [35], an apparent discrepancy is found. Despite working with the same material, these authors did not observed any meaningful shift in the non-isothermal crystallization temperature upon the application of pressure pulses (800 bar) at different undercoolings. They deduced that either no extra-nuclei were formed during the short-term pressurization, or that, if formed, they did not survive to the de-pressurization. However, the explanation of the apparent discrepancy can be that, under their experimental conditions, the extra-nuclei induced by pressure were simply undetectable. Indeed, the pressure-induced increase of nucleation density that we observe in this work is of modest entity (about 1 order of magnitude of added nuclei, for the highest pressure pulse), especially if compared to the more widely studied flow-induced nucleation phenomenon. Intuitively, the effect of an enhanced nucleation density on crystallization kinetics can be detected only if the number of extra-nuclei is at least comparable to the "reference" concentration of nuclei of the unperturbed system. This reasoning has been applied by Byelov et al. to explain the apparent ineffectiveness of flow-induced nucleation on several heterogeneously nucleated polypropylenes [20].

The nucleation density obtained in the non-isothermal crystallization of i-PP under the conditions employed by Zhang et al. [35] can be estimated to be about 7×10^{13} nuclei/m^3, using the crystallization kinetics model of van Drongelen et al. [45] (for a crystallization temperature of 115 °C and a pressure of 100 bar). This value is almost 3 orders of magnitude higher than the one measured by POM in our reference experiment at 140 °C and 100 bar. It follows that Zhang et al. did not observe any effect of pressure pulses on crystallization kinetics because the number of naturally occurring nuclei formed upon isobaric cooling from the melt overwhelmed the small increase of nuclei during the pressurization stage. Much higher pressures during the pulse would have been needed to generate a detectable number of nuclei under their experimental conditions.

5. Conclusions

A simple experimental protocol was designed to study the effect of "short-term" pressure increases (P_{pulse}) on the nucleation process of an undercooled polymer melt. The experiments, conducted on a well characterized isotactic polypropylene and for a wide range of applied pressures, showed a clear acceleration in crystallization kinetics with increasing the magnitude of the pressure during the pulse. The enhanced crystallization kinetics results from an increase in the number of nuclei as a consequence of the pressurization step. This increase of nucleation density is equal to about 1 order of magnitude for the highest pressure pulse (700 bar). The results, confirmed independently by different experimental techniques (dilatometry, on-line SAXS/WAXD and polarized optical microscopy), were explained in the light of classical nucleation theory and pressure dependence of the undercooling. However, a non-classical "barrier-less" process of nuclei formation could also be put forward. The observed effect can have a practical relevance, for the understanding and modeling of semicrystalline polymer solidification during processing. Brief pressure jumps are indeed experienced by the crystallizing polymer melt, for instance during injection molding. Moreover the proposed short-term pressure protocol opens multiple possibilities for further studies of this phenomenon. For example, investigating polymers with different pressure sensitivities of the melting point, or with different melt compressibility could help to elucidate the intimate mechanism underneath the enhanced nucleation.

Acknowledgements

This research forms part of the research programme of the Dutch Polymer Institute (DPI), project #787. NWO (Nederlandse Organisatie voor Wetenschappelijk Onderzoek) is acknowledged for providing beamtime at the ESRF. The authors are grateful to the DUBBLE (Dutch Belgian beamline) staff at the ESRF for supporting the X-ray experiments.

Appendix A. Supplementary material

Supplementary data associated with this article can be found, in the online version, at http://dx.doi.org/10.1016/j.eurpolymj.2016.11.001.

References

[1] A. Zettlemoyer, Nucleation, Marcel Dekker, New York, 1969.
[2] D.J. Blundell, A. Keller, A.J. Kovacs, J. Polym. Sci. Part B: Polym. Lett. 4 (1996) 481–486.
[3] B. Fillon, J.C. Wittmann, B. Lotz, A. Thierry, J. Polym. Sci. Part B: Polym. Phys. 31 (1993) 1383–1393.
[4] A. Ziabicki, G.C. Alfonso, Colloid Polym. Sci. 272 (1994) 1027–1042.
[5] G.C. Alfonso, A. Ziabicki, Colloid Polym. Sci. 273 (1995) 317–323.
[6] A.T. Lorenzo, M.L. Arnal, J.J. Sánchez, A.J. Müller, J. Polym. Sci. Part B: Polym. Phys. 44 (2006) 1738–1750.
[7] B.O. Reid, M. Vadlamudi, A. Mamun, H. Janani, H. Gao, W. Hu, R.G. Alamo, Macromolecules 46 (2013) 6485–6497.
[8] R.M. Michell, A. Mugica, M. Zubitur, A.J. Müller, Self-Nucleation of Crystalline Phases Within Homopolymers, Polymer Blends, Copolymers, and Nanocomposites, Springer, Berlin Heidelberg, Berlin, Heidelberg, 20161–42.
[9] M.S. Sánchez, V.B.F. Mathot, G.V. Poel, J.L.G. Ribelles, Macromolecules 40 (2007) 7989–7997.
[10] R. Androsch, H.N. Iqbal, C. Schick, Polymer 81 (2015) 151–158.
[11] E. Zhuravlev, J.W.P. Schmelzer, A.S. Abyzov, V.M. Fokin, R. Androsch, C. Schick, Cryst. Growth Des. 15 (2015) 786–798.
[12] B. Tynenska, A. Galeski, M. Kryszewski, Polym. Bull. 4 (1981) 171–177.
[13] H.L. Marand, R.S. Stein, G.M. Stack, J. Polym. Sci. Part B: Polym. Phys. 26 (1988) 1361–1383.
[14] A. Ziabicki, L. Jarecki, Macromol. Symp. 104 (1996) 65–87.
[15] Y. Yuryev, P.M. Wood-Adams, Macromol. Chem. Phys. 213 (2012) 635–642.
[16] S. Liedauer, G. Eder, H. Janeschitz-Kriegl, P. Jerschow, W. Geymayer, E. Ingolic, Int. Polym. Process. 8 (1993) 236–244.
[17] E. Koscher, R. Fulchiron, Polymer 43 (2002) 6931–6942.
[18] H. Janeschitz-Kriegl, E. Ratajski, M. Stadlbauer, Rheol. Acta 42 (2003) 355–364.
[19] M. Stadlbauer, H. Janeschitz-Kriegl, G. Eder, E. Ratajski, J. Rheol. 48 (2004) 631–639.
[20] D. Byelov, P. Panine, K. Remerie, E. Biemond, G.C. Alfonso, W.H. de Jeu, Polymer 49 (2008) 3076–3083.
[21] J.-W. Housmans, R.J.A. Steenbakkers, P.C. Roozemond, G.W.M. Peters, H.E.H. Meijer, Macromolecules 42 (2009) 5728–5740.
[22] R. Pantani, I. Coccorullo, V. Volpe, G. Titomanlio, Macromolecules 43 (2010) 9030–9038.
[23] F.D. Santis, R. Pantani, G. Titomanlio, Polymer 90 (2016) 102–110.
[24] P.C. Roozemond, M. van Drongelen, Z. Ma, A.B. Spoelstra, D. Hermida-Merino, G.W.M. Peters, Macromol. Rapid Commun. 36 (2015) 385–390.
[25] Z. Ma, L. Balzano, T. van Erp, G. Portale, G.W.M. Peters, Macromolecules 46 (2013) 9249–9258.
[26] J. He, P. Zoller, J. Polym. Sci. Part B: Polym. Phys. 32 (1994) 1049–1067.
[27] H. Ito, Y. Tsutsumi, K. Minagawa, J. Takimoto, K. Koyama, Colloid Polym. Sci. 273 (1995) 811–815.
[28] C. Angelloz, R. Fulchiron, A. Douillard, B. Chabert, R. Fillit, A. Vautrin, L. David, Macromolecules 33 (2000) 4138–4145.
[29] V. La Carrubba, V. Brucato, S. Piccarolo, J. Polym. Sci. Part B: Polym. Phys. 40 (2002) 153–175.
[30] M.H.E.V. der Beek, G.W.M. Peters, H.E.H. Meijer, Macromolecules 39 (2006) 1805–1814.
[31] T.B. van Erp, P.C. Roozemond, G.W.M. Peters, Macromol. Theory Simulat. 22 (2013) 309–318.
[32] S.A.E. Boyer, F.E.J. Fournier, C.-A. Gandin, J.-M. Haudin, Rev. Sci. Instrum. 85 (2014).
[33] R. Pantani, I. Coccorullo, V. Speranza, G. Titomanlio, Prog. Polym. Sci. 30 (2005) 1185–1222.
[34] R. Pantani, I. Coccorullo, V. Speranza, G. Titomanlio, Polymer 48 (2007) 2778–2790.
[35] L. Zhang, M.V. Drongelen, G.C. Alfonso, G.W. Peters, Eur. Polym. J. 71 (2015) 185–195.
[36] B. Wunderlich, Macromolecular Physics-Crystal Melting, vol. 3, Academic Press, 1980.
[37] J.W. Housmans, L. Balzano, D. Santoro, G.W.M. Peters, H.E.H. Meijer, Int. Polym. Process. XXIV 2 (2009) 185–197.
[38] Z. Ma, L. Balzano, G.W.M. Peters, Macromolecules 45 (2012) 4216–4224.
[39] E.M. Troisi, G. Portale, Z. Ma, M. van Drongelen, D. Hermida-Merino, G.W.M. Peters, Macromolecules 48 (2015) 2551–2560.
[40] G. Portale, D. Cavallo, G.C. Alfonso, D. Hermida-Merino, M. van Drongelen, L. Balzano, G.W.M. Peters, J.G.P. Goossens, W.J. Bras, Appl. Crystallogr. 46 (2013) 1681–1689.
[41] A.T. Jones, J.M. Aizlewood, D.R. Beckett, Die Makromol. Chem. 75 (1964) 134–158.
[42] N. Murthy, H. Minor, Polymer 31 (1990) 996–1002.
[43] H. Janeschitz-Kriegl, E. Ratajski, H. Wippel, Colloid Polym. Sci. 277 (1999) 217–226.
[44] J.R. Isasi, R.G. Alamo, L. Mandelkern, J. Polym. Sci. Part B: Polym. Phys. 35 (1997) 2945–2949.
[45] M. van Drongelen, T. van Erp, G. Peters, Polymer 53 (2012) 4758–4769.
[46] R. Campbell, P.J. Phillips, J. Lin, Polymer 34 (1993) 4809–4816.
[47] M. Avrami, J. Chem. Phys. 7 (1939) 1103–1112.
[48] J. Varga, Die Angew. Makromol. Chem. 112 (1983) 161–172.
[49] V.V. Slezov, Kinetics of First Order Phase Transitions, Wiley, 2009.
[50] R. Clausius, Ann. Phys. 155 (1850) 500–524.
[51] P.C. Roozemond, R.J.A. Steenbakkers, G.W.M. Peters, Macromol. Theory Simulat. 20 (2011) 93–109.
[52] B. Monasse, J.M. Haudin, Colloid Polym. Sci. 264 (1986) 117–122.
[53] G. Kumaraswamy, J.A. Kornfield, F. Yeh, B.S. Hsiao, Macromolecules 35 (2002) 1762–1769.